ACS APPLIED ENERGY MATERIALS

www.acsaem.org Article

Development of Porous Metal Substrate for Thin-Film Solid Oxide Fuel Cells (TF-SOFCs)

Shijie Feng,[⊥] Sangbong Ryu,[⊥] Ram Hemanth Yeerella, Ke Zhou, Quang Tuyen Tran, Sanghoon Lee, Cam Anh Thieu, Shengqiang Cai,* Nguyen Q. Minh,* and Ping Liu*

Cite This: https://doi.org/10.1021/acsaem.4c02244 Read Online

ACCESS | Metrics & More | Article Recommendations | Supporting Information

ABSTRACT: Thin-film solid oxide fuel cells (TF-SOFCs) deposited by magnetron sputtering are highly desirable due to their increased power output at reduced operating temperatures (<800 °C). Metallic porous substrates can provide mechanical support, gas supply, and current collection for TF-SOFCs and at the same time facilitate stack design, integration, and operation. A study was conducted to develop a porous metal support that is compatible with the sputtering process while offering thermal compatibility with the cell. In this study, a microporous nickel-based alloy (Inconel) modified with nanoporous nickel (NP-Ni) and yttria-stabilized zirconia (YSZ) nanoparticles has been developed as a substrate for TF-SOFCs fabricated by sputtering. Both theoretical simulations and experimental results have indicated that Inconel offers high resistance to cell bending and crack formation compared to porous nickel (Ni) substrates. A thin-film cell, less than 8 μm thick, was successfully deposited onto the Inconel substrate via sputtering. This cell demonstrated an open-circuit voltage (OCV) of 1.06 V and a peak power density of 1.07 W/cm^2 using hydrogen fuel and air at 600 °C. The cells exhibited the highest performance among metal-supported TF-SOFCs at reduced temperatures, highlighting the feasibility of combining porous metal substrates with thin-film deposition processes to produce superior-performance, reduced-temperature SOFCs.

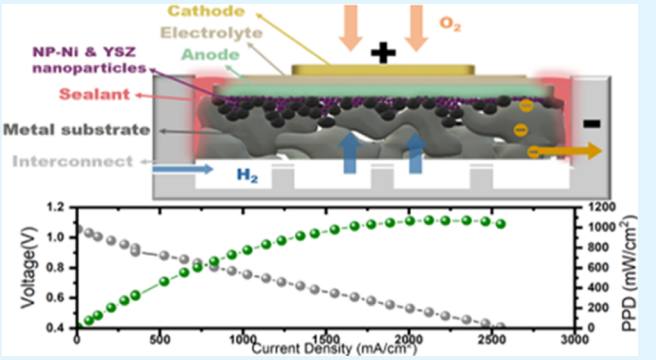

KEYWORDS: *solid oxide fuel cell, metal substrate, thin-film cell, sputtering, thermal-mechanical simulation, thermal expansion of coefficient*

INTRODUCTION

Solid oxide fuel cells (SOFCs) are highly efficient energy conversion devices with significant potential for reducing greenhouse gas emissions and enhancing energy security through the clean and efficient generation of electricity from a variety of fuels.[1−3] However, the widespread adoption of conventional SOFCs (based on oxygen ion conducting electrolytes such as yttria-stabilized zirconia or YSZ) has long been hampered by challenges such as high operating temperatures (800−1000 °C) and sluggish start-up kinetics.[4] High operating temperatures impose stringent material and processing requirements which lead to limited selection of suitable materials and manufacturing processes for cell components, interconnects, and sealants, and increased material interactions and degradation during operation. Slow start-ups make the SOFC unsuitable for certain applications such as mobile systems.[5] Therefore, developing reduced-temperature SOFCs which also allow for rapid start-up times is crucial for fully realizing the technology's potential.

One effective strategy to lower the operating temperature of YSZ-based SOFCs is to use a thin electrolyte layer, which reduces ohmic loss due to oxygen ion transport.[6] Advances in thin-film technology have enabled the fabrication of SOFCs with reduced component thicknesses (less than 5 μm) on external supports, allowing cells to operate at relatively low temperatures (500−600 °C).[7,8] For instance, atomic layer deposition (ALD)[9] has been used to fabricate a 550 nm thick YSZ electrolyte, which, when paired with a platinum electrode, delivered a peak power density of 154.6 mW/cm^2 at 450 °C.[10] Pulsed laser deposition (PLD) has been employed to deposit a bilayer electrolyte consisting of YSZ (3 μm) and GdO_2-doped ceria (GDC) (5 μm) onto a Ni-YSZ anode. Combining with $Gd_{0.5}Sr_{0.5}CoO_3$ (GSCO) cathode, the cell exhibited a peak power density of 400 mW/cm^2 at 600 °C.[11] Moreover, thin-film SOFCs (TF-SOFCs) fabricated by magnetron sputtering

Received: September 4, 2024
Revised: December 9, 2024
Accepted: December 11, 2024

on nanoporous anodic aluminum oxide (AAO) supports have demonstrated exceptional performance. For example, AAO-supported, all-sputtered cells were fabricated with a fully dense, 1.4 μm thick YSZ electrolyte layer, a fully dense, 400 nm GDC interlayer, a porous, 650 nm Ni-YSZ anode, and a porous, 600 nm lanthanum strontium cobalt iron perovskite (LSCF)-YSZ cathode (with both porous electrodes showing fibrous nanostructures). This cell configuration achieved a low area-specific resistance (ASR) of 0.25 $\Omega\cdot cm^2$ and delivered a peak power density of 1.7 W/cm^2 at 600 °C.[12] Sputtered TF-SOFC cells with lanthanum strontium cobalt perovskite (LSC)-GDC cathode even showed higher performance, a peak power density of 2.56 W/cm^2 at 600 °C.[13]

To further advance TF-SOFCs and facilitate their integration into multicell stacks and systems, it is highly desirable to use a porous, mechanically robust, electrically and thermally conducting, and thermally matching substrate.[14,15] Such a substrate would greatly simplify current collection as well as gas supply to the electrode (Figure 1). Further, such a

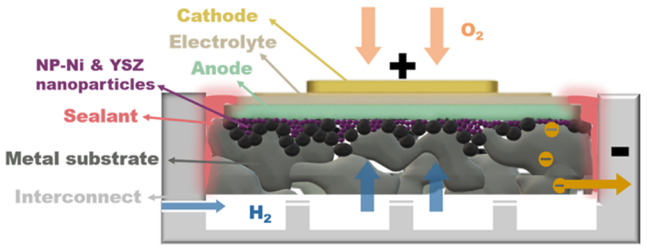

Figure 1. Schematic representation of a metal-supported thin-film SOFC.

substrate should serve as a robust structural support and offer thermal expansion match with cell components thus mitigating the risk of cell delamination and cracking[16] and facilitating fast start-up. Porous metals meeting those characteristics thus are preferable for use as substrates for TF-SOFCs. Previous work has demonstrated the capability of porous metal substrates to support conventional SOFCs fabricated by techniques such as screen printing[17,18] or spin coating.[19] For example, an Fe−Cr alloy-supported SOFC was fabricated with a thin YSZ electrolyte (2 μm) with electrodes (Ni-YSZ anode and LSC cathode) of about 100 μm thick. The cell achieved above 1.7 W/cm^2 power density at 650 °C and 0.7 V.[20] However, this high-performance SOFC still incurs high fabrication costs due to the need for high-temperature sintering (>1000 °C). Sputtering, on the other hand, can be used for making TF-SOFCs at room temperature.[12,13] However, to enable the use of a sputtering process to deposit all cell layers in thin-film forms on porous metal substrates, the substrate needs to have very low surface roughness and a uniform nanoporous structure at the surface.

Herein, we first construct a thermal model to show that porous Inconel substrates, in contrast to nickel, exhibit remarkable thermal stability, resisting TF-SOFC bending and crack propagation along the interfaces. Following this modeling study, a porous Inconel substrate was designed and fabricated with a nanoscale surface roughness of 138 nm. Achieved by nanoporous nickel (NP-Ni) and YSZ nanoparticle infiltration and uniaxial compression, this surface smoothness is crucial for supporting the TF-SOFC structure and cell fabrication by sputtering. A thin-film SOFC, with a total thickness of less than 8 μm and featuring an approximately 2 μm thick YSZ electrolyte layer, was subsequently deposited onto the modified Inconel substrate. The schematic shown in Figure 1 illustrates the cell configuration. The cell exhibited an open-circuit voltage (OCV) of ∼1.06 V and achieved a peak power density of 1.07 W/cm^2 at 600 °C with hydrogen fuel. By combining a porous metal substrate with thin-film sputtering deposition of the cell components, this cell outperformed other metal-supported SOFCs (Figure S10).

EXPERIMENTAL SECTION

Measurement of Mechanical Properties. Nanoindentation tests were conducted on porous Ni, Inconel, and sputtered yttria-stabilized zirconia (YSZ) samples to determine their mechanical properties by using an iMicro instrument (KLA, Inc.) equipped with a Berkovich tip (Type TB30524) capable of applying a maximum load of 50 mN. A constant strain rate of 0.1 s^{-1} was applied. The test proceeded until the target indentation load was achieved. The InView software (RunTest and ReviewData modules) facilitated testing and subsequent data analysis. Thermal drift remained below 0.05 nm/s throughout the testing process. Due to the inhomogeneity of the materials, multiple locations (12−15) were probed on each sample.

Measuring Coefficient of Thermal Expansion (CTE) Using Dynamic Mechanical Analysis (DMA). The CTE of NP-Ni and Inconel was measured using the Iso Strain Temperature ramping procedure on a DMA instrument (RSAG2) with a maximum temperature capacity of ∼22 °C. Samples, each with a diameter of 10 mm and a height of 1 mm, were subjected to an initial compression of 1%. The temperature was increased at a rate of 0.2 °C/min from 20 to 22 °C. Given that the SOFC operating temperature (600 °C) is well below the melting and sintering points (>1400 °C) of the substrates, we consider CTE behavior to be linear within the operational temperature range.[21,22] Moreover, since both substrates were tested under identical conditions, we assume that their thermal expansion trends are consistent across the relevant temperature range. Accordingly, our low-temperature CTE approximation provides a reasonable estimate for this study. Testing and data analysis were conducted by using TRIOS software. We note that our approach in evaluating CTE was taken due to instrument limitations. Ideally, a standard CTE measurement (dilatometry and thermal-mechanical analysis, TMA) at the operational temperature of the SOFCs is preferred.

Since the samples were constrained at the prescribed compression, the thermal strains caused the force to increase. We measured the steady-state force before and after temperature ramping to calculate the CTE of the material.

$$\mathrm{CTE} = \Delta F/(A^*E^*\Delta T)$$

where F is the thermal expansion force, E is Young's modulus, A is the cross-sectional area, and ΔT is the change in temperature.

Finite Element Simulation Modeling. We constructed a two-dimensional (2D) model in ABAQUS 2022, as shown in Figure 2a, consisting of a YSZ electrolyte and Ni-YSZ anode layer on top of the metal substrate base.

The fuel cell was treated as a stack of rectangular slabs. The cross section of the fuel cell was considered along the $Z-X$ plane at $Y = 0$. Since this cross section had symmetry along the Z-axis, we modeled only half of it in our finite element method (FEM) analysis, enforced symmetry boundary condition along $X = 0$, and also constrained the single node near at origin (0, 0, 0), on the bottom edge of the metal substrate.

We first performed a simple thermal deformation analysis by ramping the temperature of the whole stack from 300 to 900 K, and we observed the extent of bending as a result of CTE mismatch. The model did not account for the microstructural details of each component. Instead, each layer was defined using its effective elastic modulus and CTE, both measured at room temperature.

Later, we introduced cracks along the interfaces of the anode/YSZ electrolyte and the anode/metal substrate, near the free ends. In

https://doi.org/10.1021/acsaem.4c02244
ACS Appl. Energy Mater. XXXX, XXX, XXX−XXX

general, when the crack size is minimal, the driving force for crack growth is proportional to the crack size; however, beyond a certain threshold, it becomes independent of the crack size. In this study, the crack length was set to 5% of the layer width, allowing for a significant difference in the driving forces between the two metal substrates to be observed. The crack propagation was specified to occur in the inward ($-x$) direction. We calculated the energy release rate for crack propagation (J-integral) as the temperature increased from 300 to 900 K. The greater the value of J-integral was, the higher the risk of crack propagation became.

The layer's elastic properties were obtained from the results of nanoindentation tests, and CTE was calculated from the DMA tests. The approximate global mesh size of 25 μm, at least 5 elements along the thickness of YSZ layers, and free meshing technique were used to discretize the parts. CPS8, an eight-node quadrilateral mesh element within the standard element library from the family of plane stress with quadratic geometric order, was chosen as the mesh element type for all of the layers, except near the crack tip. CPS6, 6-node quadratic plane stress triangular mesh elements with the sweep meshing technique, were used near the region of the crack tip, with appropriate mesh size and default settings. Nonlinear geometric effects are considered in the step. Default settings were used for the step solver and the solution techniques. Table S1 gives the material parameters for modeling and the dimensions of each layer. We modeled these layers as fully elastic materials without plasticity and allowing for thermal strains.

Nanoporous Nickel (NP-Ni) Synthesis. Unless otherwise stated, all commercial reagents and solvents were used as purchased without additional purification. Nanoporous nickel (NP-Ni) powder was synthesized through a conversion reaction synthesis process. For example, 1 g of $NiCl_2$ was dispersed in 10 mL of hexane. Next, *n*-butyl lithium (1.25 times the stoichiometric excess) was added dropwise to the dispersion, and the resulting mixture was stirred at room temperature for 24 h. The nanocomposite powder was then separated by filtration and washed with 30 mL of methanol to remove LiCl. The resulting black Ni powder was dried under an argon atmosphere. A postannealing process was performed to slightly sinter the NP-Ni under argon and prevent oxidation in ambient air. All synthesis procedures were conducted in an argon glovebox with $\leq$0.5 ppm of O_2 and <0.5 ppm of H_2O.

Porous Ni and Porous Inconel Substrate Fabrication. NP-Ni powder was pelletized using a 1/2 in. pressing die set under 100 MPa pressure, then sintered at 600 °C in a reducing atmosphere (3% H_2 in Ar), producing a circular substrate with an area of 1.2 cm^2 and a thickness of 0.2 mm. A commercial Inconel 600 filter (8.5 in. × 10 in., Mott Corporation) was cut into pieces of 1 cm × 1 and 2.5 cm × 2.5 cm, each with a thickness of 1 mm. In terms of the infiltration step, NP-Ni, with an approximate particle size of 1 μm, was synthesized and dispersed in ethanol at a concentration of 2 g/mL. A vacuum line was connected directly to one side of the Inconel substrate, and 3 mL of the NP-Ni dispersion was applied, infiltrating the micrometer-sized pores on the opposite side. Following this, a dispersion of 100 nm YSZ nanoparticles at a concentration of 1 g/mL was introduced using the same filtration method to reduce the surface roughness. The substrate was then compressed using a uniaxial press at ~150 MPa and sintered at 700 °C under a reducing atmosphere (3% H_2 in Ar) to integrate all components onto the surface.

Thin-Film Cell Fabrication. The TF-SOFC in this study was fabricated on metal supports by utilizing a sputtering machine (AJA International Inc.). Sputtering offers a cost-effective, material-efficient, and time-efficient alternative to traditional manufacturing processes for the SOFC. A preliminary cost assessment for metal-supported thin-film SOFC showed a stack capital cost of $56/kW, significantly lower than the current cost of $250 $/kW for conventional SOFC stacks.[23] This is due to the much more efficient use of materials during sputtering compared to conventional slurry casting processes. Sputtering also eliminates the long (several days) and high temperature (up to 1400 °C) sintering that is required for electrolyte and electrode layer fabrication. Additional details comparing sputtering with conventional processes are provided in the SI.

During the sputtering, each component, Ni-YSZ, YSZ, gadolinium doped ceria (GDC), and lanthanum strontium cobalt perovskite (LSC)-GDC was deposited sequentially as the anode, electrolyte, barrier layer, and cathode, respectively. For the anode, a 3 in. Ni target (Kurt J. Lesker Company) and a 2 in. Y−Zr metal alloy target (Y/Zr 0.15/0.85 atom %, Advanced Engineering Materials Limited, China) were co-sputtered at 30 mTorr, 200 W, and 300 °C for 4 h. The YSZ electrolyte was deposited using a 3 in. 8 mol % Y_2O_3 doped ZrO_2 target (YSZ, Advanced Engineering Materials Limited, China) at 3 mTorr, 150 W, and room temperature for 9 h, while the GDC barrier layer was deposited with a 3 in. 20 mol % Gd_2O_3 doped CeO_2 target (GDC20, Advanced Engineering Materials Limited, China) at 2 mTorr and 200 W for 1 h. The cathode, LSC-GDC, was deposited by a co-sputtering process using 2 in. $(La_{0.6}Sr_{0.4})_{0.98}Co_{1.8}O_x$ (LSC, Advanced Engineering Materials Limited, China) and 3 in. Gd−Ce alloy target (Gd/Ce 0.8/0.2 atom %, Advanced Engineering Materials Limited, China) at 30 mTorr and room temperature for 150 min with power conditions of 200 and 30 W for LSC and Gd−Ce, respectively. For both substrates, the anode and electrolyte were sputter-coated across the entire substrate surface in sequence. The active cell area was determined by the cathode. A mask with a fixed area of 3 mm^2 was used during fabrication for both substrates, resulting in an active cell area of 3 mm^2.

Electrochemical Characterization. The cell was mounted on a custom-made test stand. Silver paste and a gold mesh were used as a current collector for the anode and cathode, respectively. A MgO sealant (Aremco), was applied to the cell after curing the silver paste. To operate the cell, the cell was heated to 600 °C at a rate of 20 °C/min. During the temperature ramp, a 100 sccm flow of 3% humidified nitrogen/hydrogen mixture gas (N_2/H_2 90/10%) was introduced to the anode side, while the cathode side was exposed to ambient air. Upon reaching the operating temperature, the proportion of hydrogen in the anode side gas was gradually increased to 100% hydrogen with 3% humidity. Electrochemical impedance spectroscopy (EIS) measurements were conducted using a Gamry Reference 3000 (Gamry Instruments). The measurements were performed over a frequency range of 10^6−1 Hz with a perturbation amplitude of 30 mV rms. The ionic conductivity was calculated based on Ohm's Law. Current−voltage-power (I−V−P) curves were also obtained using a Gamry Reference 3000 with a scan rate of 25 mV/s.

RESULTS AND DISCUSSION

Thermomechanical Modeling to Define Required Metal Substrate Property. A metal substrate for the SOFC must possess several key attributes, including compatibility (chemical and thermal) with cell components, mechanical strength, thermal stability, high thermal and electrical conductivity, and cost-effectiveness. The metal should be suitable to be formed into substrates with the required dimensions and porous microstructure. Nickel (Ni) is a well-known material used in SOFC anodes, meeting most of these criteria for use as a substrate in the anode environment. Additionally, Ni substrates can be beneficial in support of the anode reactions as Ni exhibits excellent catalytic activity in the electro-oxidation of hydrogen fuel.[24] Nickel substrates were thus first considered in this study. Consequently, Ni substrates, characterized by micrometer-sized pores, were fabricated (Figure S1), with details of the synthesis method provided in the Experimental Section. To assess the mechanical properties of the substrate, nanoindentation and dynamic mechanical analysis were employed to measure the elastic modulus and coefficient of thermal expansion (CTE), respectively, with the results shown in Figure S2. The results show that porous Ni substrate exhibits an elastic modulus of 15 GPa and a CTE of 4 ppm/°C. The modulus value is significantly lower than the one of bulk Ni (elastic modulus ~200 GPa) due to the inherent characteristics of porous materials. The presence of pores

https://doi.org/10.1021/acsaem.4c02244
ACS Appl. Energy Mater. XXXX, XXX, XXX−XXX

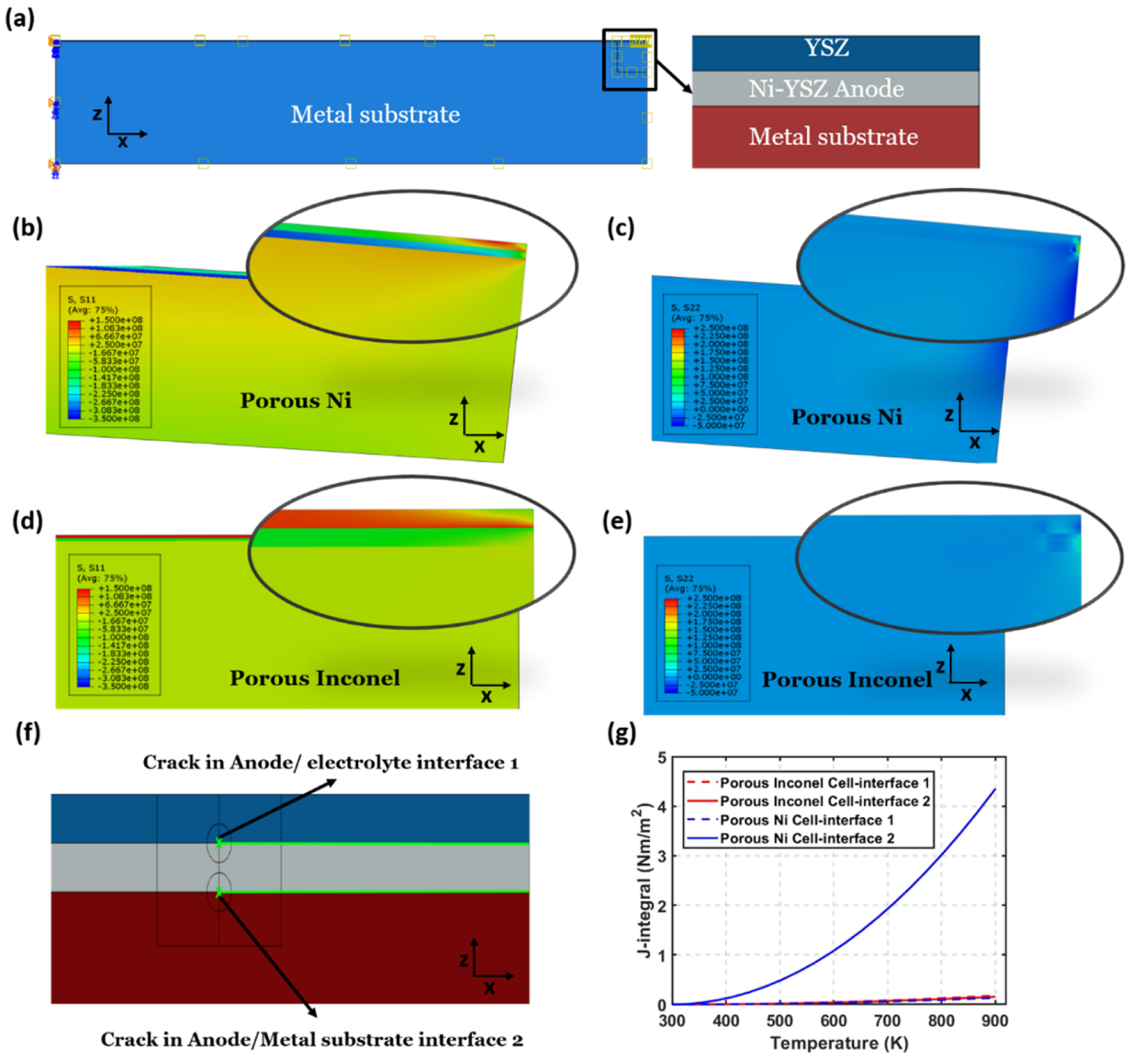

Figure 2. Finite element simulation for Ni- and Inconel-supported cells. (a) ABAQUS model depiction; (b, d) distribution of normal stress in the horizontal direction for Ni- and Inconel-supported cells, respectively, at 900 K; (c, e) distribution of normal stress in the vertical direction for Ni- and Inconel-supported cells, respectively, at 900 K; zoom-in images of stress distribution present on the right top of each image; (f) finite element method (FEM) analysis of crack propagation at YSZ/Ni-YSZ interface 1 and Ni-YSZ/metal substrate interface 2. (g) Energy release rate (J-integral) at different interfaces.

reduces stiffness, allowing deformation with less resistance. This is particularly evident when sintering is minimal, as the pore network can rearrange under stress, further lowering the effective modulus. Additionally, the CTE value, much lower than that reported for bulk Ni,[21] is attributed to slight sintering of NP-Ni during heating; the highly porous nanostructural network undergoes pore rearrangement, resulting in less thermal expansion at elevated temperature.

We next employed finite element simulation to evaluate the feasibility of the porous Ni substrate. The cell configuration used in this simulation comprised a porous Ni substrate as the bottom support layer with a Ni-YSZ anode and thin YSZ electrolyte layers stacked successively on top (Figure 2a). All of the layers were modeled strictly as elastic materials, devoid of plastic deformation while accommodating thermal expansion. All of the layer dimensions and material properties are listed in Table S1. Poisson's ratio values were selected from the existing literature,[25] while Young's modulus and CTE were directly taken as the measured values of elastic modulus and thermal expansion, respectively (Figure S2). Subsequently, a single-step finite element method (FEM) analysis was conducted, tracking the bending behavior of the entire structure as the temperature increases from 300 to 900 K. It was observed that the use of porous Ni as the metal substrate induced significant bending (see Figure 2b,c). This effect is due to the difference in the CTE (4 ppm/°C of porous Ni vs 10.5 ppm/°C of YSZ), which creates a high-stress gradient within the structure. The thin-film layers are subjected to compressive stress, likely leading to the propagation of microcracks through the thickness of cell components and delamination between the thin-film cell and Ni substrate.[26] This bending behavior is indeed observed experimentally, as shown in Figure S3. Both theoretical analysis and experimental findings underscore the necessity for an alternative metal substrate with improved thermal expansion compatibility and thermal stability.

Inconel 600, a nickel-based alloy, has been identified as a promising candidate for metallic interconnections in SOFCs owing to its exceptional thermal-mechanical performance and resistance to oxidation.[27] The CTE of bulk Inconel 600 (13.3 ppm/°C)[22] is much smaller than that of bulk Ni (~17 ppm/°C)[21] and closely aligns with that of YSZ electrolyte (~10.5 ppm/°C).[28] This alignment helps to mitigate stresses induced

https://doi.org/10.1021/acsaem.4c02244
ACS Appl. Energy Mater. XXXX, XXX, XXX−XXX

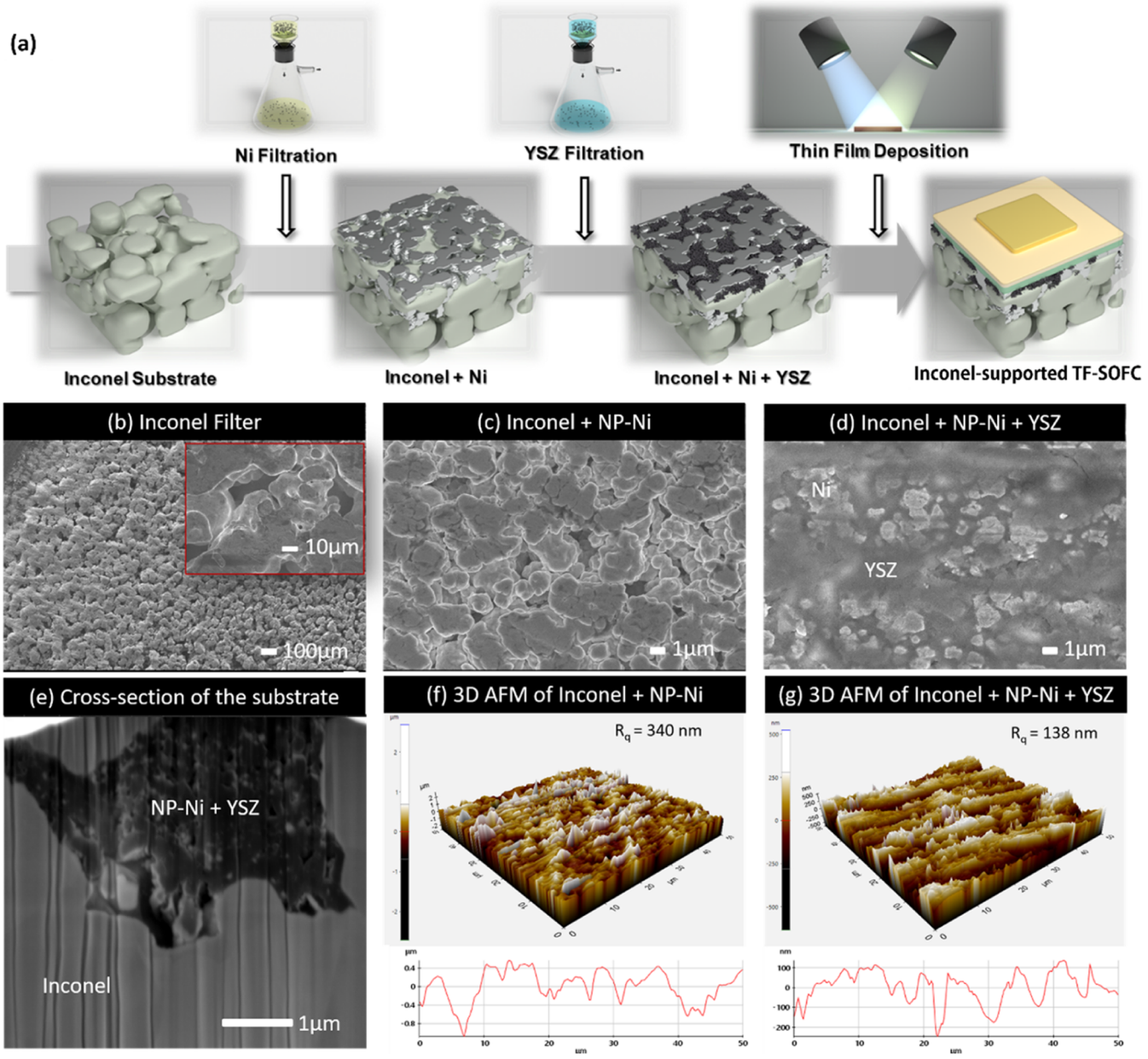

Figure 3. (a) Schematic diagram of the process of modifying Inconel substrate and fabricating supported thin-film SOFC. (b) Surface morphology of porous Inconel; (c) surface morphology of Inconel after NP-Ni infiltration; (d) surface morphology of Inconel after NP-Ni and YSZ nanoparticles infiltration; (e) cross-sectional view of modified substrate; (f) three-dimensional (3D) atomic force microscopy (AFM) image of surface of Inconel after NP-Ni infiltration; (g) 3D AFM image of surface of Inconel after NP-Ni and YSZ nanoparticles infiltration.

by the CTE mismatch when integrating with a thin-film YSZ electrolyte. Consequently, Inconel was selected for our initial thin-film SOFC prototype. A commercially available porous Inconel 600, featuring microsized pores, was obtained. Utilizing the measured elastic modulus (5 GPa) and CTE (12 ppm/°C) of the porous Inconel substrate (see Figure S4), the model revealed minimal bending and uniform stress distribution within the fuel cell structure in both x and z directions (as depicted in Figure 2d,e), thereby reducing the risk of failure. Subsequently, FEM analysis was conducted to observe crack propagation along the interfaces of the electrolyte/anode and anode/metal substrate (Figure 2f,g). The driving force for crack propagation, represented by the J-integral, was computed as the cracks extended inward (negative x direction) with increasing temperature from 300 to 900 K for porous Ni (blue) and Inconel (red) as metal substrates. The crack will propagate once the driving force exceeds the fracture toughness of the respective interfaces. The interface of Ni-YSZ/YSZ is termed Cell-interface 1 and plotted in a dotted line, and Cell-interface 2 corresponds to the YSZ/Metal substrate boundary, plotted as a solid line. According to the simulation, the J-integral values for crack growth were found to be highest at the porous Ni substrate and Ni-YSZ anode interface, primarily due to the significant difference in CTE between the substrate and the cell components. Conversely, porous Inconel as the metal substrate resulted in a substantially lower crack driving force at both anode/electrolyte and anode/substrate interfaces compared to Ni. The results presented here are from simulations with varying thicknesses of porous Ni and porous Inconel 600 layers, using

https://doi.org/10.1021/acsaem.4c02244
ACS Appl. Energy Mater. XXXX, XXX, XXX−XXX

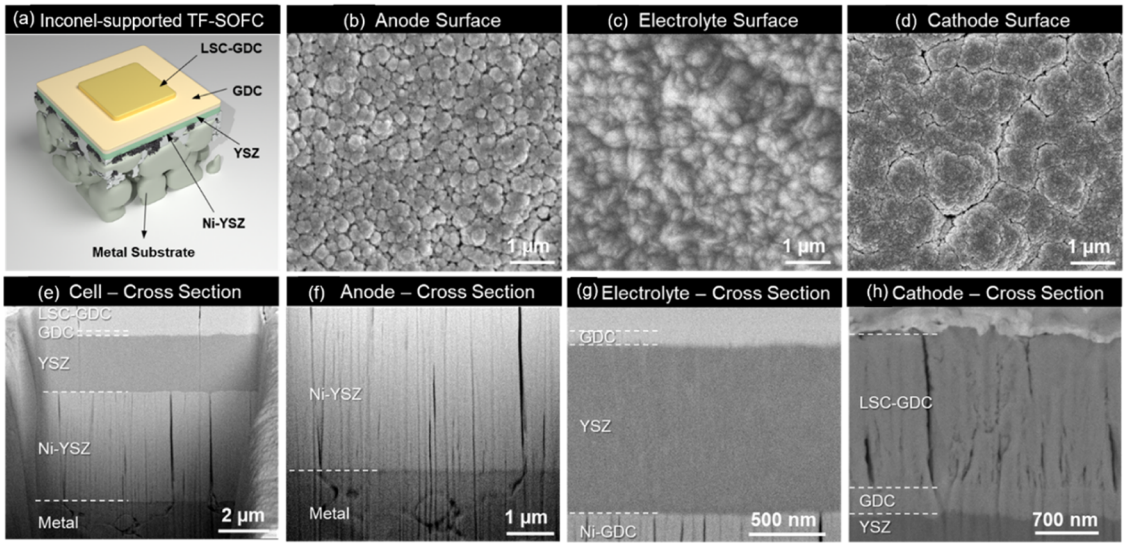

Figure 4. (a) Schematic configuration of the metal-supported TF-SOFC (not in scale); (b) SEM of Ni-YSZ anode surface; (c) SEM of YSZ electrolyte surface; (d) SEM of LSC-GDC cathode surface; (e) cross-sectional SEM of full cell; (f) cross-sectional SEM of Ni-YSZ; (g) cross-sectional of YSZ; (h) cross-sectional SEM of LSC-GDC.

the same dimensions as those in the experimental tests. We also ran simulations with an Inconel layer of reduced thickness, equivalent to that of the porous Ni layer, but the results were similar to those obtained with thicker Inconel layers. The simulation outcomes indicate that a porous Inconel substrate is better suited to support TF-SOFCs, as the cell exhibits enhanced resistance to crack propagation due to its relatively compliant nature and closely matched CTE.

Fabricating Inconel Substrate Suitable for Thin-Film Deposition. To facilitate the sputtering deposition of thin-film cell components (less than 10 μm) on a macroporous Inconel substrate (characterized by pores of tens of micron meters in size as depicted in Figure 3b), several surface treatments were employed to decrease both pore size and surface roughness (shown in Figure 3a).

The first treatment was to fill the macroporous Inconel with nanoporous Ni particles (~800 nm). Following our previously published procedure, nanoporous Ni particles were synthesized via a conversion reaction method where $NiCl_2$ is reduced with butyl lithium forming a nanocomposite of Ni and LiCl followed by dissolution of LiCl using methanol.[29,30] The nanoporous Ni particles were dispersed in ethanol and infiltrated into the macropores on the Inconel surface. Following uniaxial compression and thermal treatment at 700 °C under $Ar-H_2$ atmosphere, the surface was modified to contain pores of a few micrometers in size with a root-mean-square (RMS) roughness of 340 nm (illustrated in Figure 3c,f). The Ni-YSZ anode and YSZ electrolyte layers were then deposited onto the Ni-modified Inconel (Inconel-Ni) surface, as shown in Figure S5. The resulting uneven surface of the Inconel substrate along with pinholes formed within the YSZ layer were probably the root causes of the observed cell shorting at elevated temperatures, highlighting the necessity for further surface refinement.

The second treatment was then used to further even out the surface of substrate. In this step, YSZ nanoparticles (<100 nm) were infiltrated into the Inconel-Ni surface utilizing the same methodology as that used for NP-Ni particles. YSZ was chosen due to its exceptional thermal stability and effectiveness in preventing Ni nanoparticles agglomeration.[31] After compacting and sintering at 700 °C, surface morphology (Figure 3d) and cross-sectional analysis of the substrate via focused ion beam (FIB) scanning electron microscopy (SEM) showed that both nanoporous Ni and YSZ nanoparticles filled the surface pores of Inconel (Figure 3e). Energy-dispersive spectroscopy (EDS) analysis verified the exclusive presence of YSZ on the substrate surface (Figure S6). The second treatment resulted in nanoscale pores at the surface (Figures 3d and S7) and showed a significantly reduced RMS roughness of 138 nm (Figure 3g) for the Inconel substrate, indicating an improved surface suitable for thin-film sputter deposition.

Sputtering TF-SOFC Cell on Porous Inconel Substrate. Figure 4a shows a schematic of an SOFC cell deposited on a porous Inconel substrate. The fabrication process involved the sequential sputtering of a Ni-YSZ anode, YSZ electrolyte, GDC interlayer, and LSC-GDC cathode within the same chamber, designated as LSC-GDC/GDC/YSZ/Ni-YSZ. Detailed microstructural characterizations of each layer were performed, with the findings depicted in Figure 4. The specific sputtering parameters are detailed in the Experimental Section.

To fabricate a full cell, a porous Ni-YSZ anode with a thickness of approximately 4 μm was first deposited on an Inconel substrate. Examination of the surface morphology of the anode, shown in Figure 4b, reveals nanosized particles with an average size of 90 nm clustering together to form fine pores. This microstructure is advantageous, providing a high surface area for reactive sites and facilitating the mass transport of H_2.[32] The connectivity of these pores is confirmed by the cross-sectional image of the anode (Figure 4f). Subsequently, a YSZ electrolyte layer, approximately 2 μm thick, was deposited on top of the Ni-YSZ layer. Observations of both the surface (Figure 4c) and cross section (Figure 4g) reveal the absence of pores, indicating a fully dense structure. Following the YSZ layer, a dense GDC layer (illustrated in Figure 4g,h) was deposited to serve as an interlayer between the electrolyte and cathode, aimed at preventing side reactions between the YSZ electrolyte and LSC cathode.[33] The final layer, a ~ 1.7 μm thick LSC-GDC cathode, was then deposited, featuring a columnar microstructure with relatively larger grain sizes and similar pore sizes (<100 nm) in comparison to the anode.

https://doi.org/10.1021/acsaem.4c02244
ACS Appl. Energy Mater. XXXX, XXX, XXX−XXX

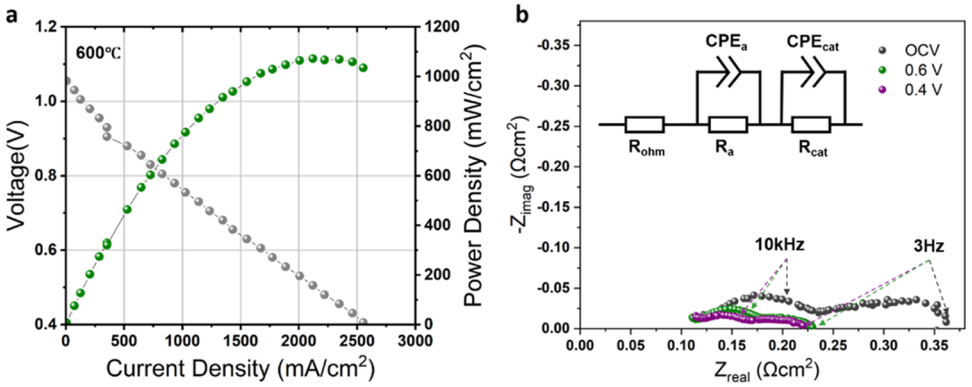

Figure 5. (a) Current−voltage (I−V) and current−power (I−P) curves; (b) EIS measurements of porous Inconel-supported TF-SOFCs at different voltages with H_2 fuel and air at 600 °C.

Figure 4e shows a cross-sectional image of the complete cell structure, highlighting the distinct microstructures that have been successfully deposited on the Inconel substrate via magnetron sputtering.

Demonstrating Cell Performance. The Inconel-supported TF-SOFC cell underwent electrochemical testing with 97% hydrogen, 3% H_2O as the fuel, and air as the oxygen source. The cell was heated at a rate of 20 °C per minute without any issues. The cell achieved an open-circuit voltage (OCV) of approximately 1.06 V at 600 °C (Figure 5a). The deviation from the theoretical OCV (1.13 V) at 600 °C[34] could be attributed to structural defects and inadequate sealing. We are actively investigating this issue and working toward resolving it. The cell exhibited a peak power density of 1.07 W/cm^2 at 600 °C over a 3 mm^2 active area, marking the highest performance recorded for metal-supported TF-SOFCs with an electrolyte thickness of less than 10 μm. This study marks our initial exploration into fully thin-film, metal-supported SOFCs. A small active area (3 mm^2) was employed to ensure controlled and reproducible testing, a method commonly adopted in foundational research on thin-film SOFC development.[35−37] Previous studies have shown comparable power density between large-area cells (16 cm^2) and small-area cells (<1 cm^2), indicating that results obtained from small-area cells are relevant for larger-scale applications.[38] To further ensure reliability, we fabricated another cell with an identical configuration and active area. This additional cell was safely tested under a lower ramping rate of 2 °C/min, as shown in Figure S8. The cell delivered a consistent peak power density of approximately 1.02 W/cm^2, confirming the reproducibility of our performance results and indicating that our Inconel substrate can support rapid start-up without noticeable damage or performance degradation.

For comparison, a porous Ni-supported TF-SOFC was also fabricated (Figure S9c) and tested. This cell delivered a peak power density of approximately 175 mW/cm^2 at 550 °C (Figure S9b) but was short-circuited at temperatures above 550 °C (Figure S9a). Post-mortem characterization (Figure S9d) showed delamination of the YSZ electrolyte layer from the anode, likely due to the thermal-mechanical stress-induced bending, consistent with the simulation results. Due to its mechanical compliance and a CTE close to that of YSZ, porous Inconel demonstrated superior mechanical stability as a substrate compared to porous Ni. Additionally, a comparison of our Inconel-supported cell with other reported metal-supported SOFCs in terms of thickness and power density is shown in the SI (Figure S10). As shown in Figure S10, the Inconel-supported SOFC with the thin-film cell made by sputtering has the lowest cell thickness (<8 μm) while delivering the highest power density (>1 W/cm^2).

Electrochemical impedance spectroscopy (EIS) measurements, detailed in Figure 5b, were conducted at different cell voltages (OCV, 0.6 V, 0.4 V) at 600 °C. The ohmic resistance and electrode polarization resistance were extracted from the EIS data by fitting with the equivalent circuit (resistances, R and constant phase elements, CPE) shown in Figure 5b. The individual fitting results are presented in Figure S11 for further clarity. Due to the thin-film electrolyte configuration, the cell's ohmic resistance remained low at approximately 0.1 Ω·cm^2, independent of cell voltage. From this value, an ionic conductivity of 2 × 10^{-3} S/cm was calculated, aligning closely with the standard sintered YSZ, which typically exhibits an ionic conductivity of around 10^{-3} S/cm at 600 °C.[39,40] This result highlights the efficacy of sputtering technology in producing dense and uniform electrolytes and demonstrates its potential for integration with metal substrates without compromising the ion conductivity. Based on the impedance fitting at OCV, the anode polarization resistance (R_a) and cathode polarization resistance (R_{cat}) were 0.14 and 0.13 Ω·cm^2, respectively. At 0.6 V, R_a and R_{cat} decreased to 0.07 and 0.06 Ω·cm^2, respectively. Further decreases were observed at 0.4 V, with 0.06 Ω·cm^2 for the anode and 0.05 Ω·cm^2 for the cathode. These low electrode polarization resistances were attributed to the nanoscale grain size of electrodes, obtained by sputtering, which created a high concentration of triple-phase boundaries (TPBs), thus enhancing reaction kinetics.[41] Finally, cells with a larger active area of 1 cm^2 were fabricated by using the same sputtering procedure. These cells achieved a peak power density of approximately 0.67 W/cm^2 (Figure S12) at 600 °C which was lower than that obtained for cells with smaller areas. The I−V curve indicates that the reduced performance was primarily due to inadequate current collection on the cathode side and gas concentration polarization.[42,43] Specifically, ohmic resistance increased at the cell edges as the cell size increased. Additionally, the larger quantity of Ni and YSZ used to ensure adequate pore closure in the 2.5 cm × 2.5 cm substrate may have unintentionally reduced porosity in certain areas, potentially limiting the hydrogen supply to the electrode surface. These findings suggest that comparable performance could be achieved with further optimization of current collection methods and substrate porosity/microstructure during fabrication scale-up.

https://doi.org/10.1021/acsaem.4c02244
ACS Appl. Energy Mater. XXXX, XXX, XXX−XXX

Specifically, stainless steel represents a cost-effective alternative to Inconel, while offering a closer CTE to YSZ. Our results obtained on Inconel, however, demonstrate the potential of a metal-supported SOFC fabricated by a sputtering process.

CONCLUSIONS

Guided by thermomechanical simulations, porous Inconel is selected as a substrate for TF-SOFCs. Use of this metal substrate lowers cell bending stresses at elevated temperatures, resulting in reduced risks of cell crack formation. By applying infiltration and mechanical compression for surface modifications, we fabricated a porous Inconel substrate with nanoscale pores at the surface and a reduced surface roughness of 138 nm. A thin-film SOFC cell (LSC-GDC cathode/GDC interlayer/YSZ electrolyte/Ni-YSZ anode) was deposited on the modified Inconel substrate by using sputtering. The cell was heated at a fast start-up rate of 20 °C/min to the operating temperature of 600 °C without any issues and achieved an open-circuit voltage (OCV) of 1.06 V and a peak power density of 1.07 W/cm^2 using hydrogen fuel and air at 600 °C. The demonstration of a thin-film SOFC supported on an external metal substrate highlights an optimal configuration for TF-SOFCs, offering superior areal and weight-specific power densities, which is crucial for weight-sensitive applications.

ASSOCIATED CONTENT

Supporting Information

The Supporting Information is available free of charge at https://pubs.acs.org/doi/10.1021/acsaem.4c02244.

Finite element simulation details, coefficient of thermal expansion data, nanoindentation data, energy-dispersive spectroscopy data, atomic force microscopy data, and extra full cell data (PDF)

AUTHOR INFORMATION

Corresponding Authors

Shengqiang Cai − *Department of Mechanical and Aerospace Engineering, University of California San Diego, La Jolla, California 92093, United States;* orcid.org/0000-0002-6852-7680; Email: s3cai@ucsd.edu

Nguyen Q. Minh − *Center for Energy Research, University of California San Diego, La Jolla, California 92093, United States;* orcid.org/0000-0003-3276-6150; Email: nminh@ucsd.edu

Ping Liu − *Materials Science and Engineering Program, University of California San Diego, La Jolla, California 92093, United States; Aiiso Yufeng Li Family Department of Chemical and Nano Engineering, University of California San Diego, La Jolla, California 92093, United States;* orcid.org/0000-0002-1488-1668; Email: piliu@ucsd.edu

Authors

Shijie Feng − *Materials Science and Engineering Program, University of California San Diego, La Jolla, California 92093, United States;* orcid.org/0000-0001-5797-8542

Sangbong Ryu − *Center for Energy Research, University of California San Diego, La Jolla, California 92093, United States;* Present Address: Pacific Northwest National Laboratory, Richland, Washington 99352, United States

Ram Hemanth Yeerella − *Department of Mechanical and Aerospace Engineering, University of California San Diego, La Jolla, California 92093, United States;* orcid.org/0000-0002-9344-6313

Ke Zhou − *Aiiso Yufeng Li Family Department of Chemical and Nano Engineering, University of California San Diego, La Jolla, California 92093, United States*

Quang Tuyen Tran − *Center for Energy Research, University of California San Diego, La Jolla, California 92093, United States*

Sanghoon Lee − *Center for Energy Research, University of California San Diego, La Jolla, California 92093, United States;* orcid.org/0000-0002-1568-5028

Cam Anh Thieu − *Center for Energy Research, University of California San Diego, La Jolla, California 92093, United States*

Complete contact information is available at: https://pubs.acs.org/10.1021/acsaem.4c02244

Author Contributions

⊥S.F. and S.R. contributed equally to this work.

Notes

The authors declare no competing financial interest.

ACKNOWLEDGMENTS

This work was funded by the U.S. Department of Energy/Advanced Research Project Agency-Energy (ARPA-E) under the Cooperative Agreement DE-AR0001347.

REFERENCES

(1) Minh, N. Solid oxide fuel cell technology features and applications. *Solid State Ionics* **2004**, *174* (1−4), 271−277.

(2) Corigliano, O.; Pagnotta, L.; Fragiacomo, P. On the technology of solid oxide fuel cell (SOFC) energy systems for stationary power generation: A Review. *Sustainability* **2022**, *14* (22), 15276.

(3) Ormerod, R. M. Solid oxide fuel cells. *Chem. Soc. Rev.* **2003**, *32* (1), 17−28.

(4) Singh, M.; Zappa, D.; Comini, E. Solid oxide fuel cell: Decade of progress, future perspectives and challenges. *Int. J. Hydrogen Energy* **2021**, *46* (54), 27643−27674.

(5) Zakaria, Z.; Awang Mat, Z.; Abu Hassan, S. H.; Boon Kar, Y. A review of solid oxide fuel cell component fabrication methods toward lowering temperature. *Int. J. Energy Res.* **2020**, *44* (2), 594−611.

(6) Zhang, J.; Ricote, S.; Hendriksen, P. V.; Chen, Y. Advanced materials for thin-film solid oxide fuel cells: Recent progress and challenges in boosting the device performance at low temperatures. *Adv. Funct. Mater.* **2022**, *32* (22), No. 2111205.

(7) Chasta, G.; Himanshu; Dhaka, M. S. A review on materials, advantages, and challenges in thin film based solid oxide fuel cells. *Int. J. Energy Res.* **2022**, *46* (11), 14627−14658.

(8) Yang, Y.; Zhang, Y.; Yan, M. A review on the preparation of thin-film YSZ electrolyte of SOFCs by magnetron sputtering technology. *Sep. Purif. Technol.* **2022**, *298*, No. 121627.

(9) Shin, J. W.; Oh, S.; Lee, S.; Go, D.; Park, J.; Kim, H. J.; Yang, B. C.; Cho, G. Y.; An, J. ALD CeO2-Coated Pt anode for thin-film solid oxide fuel cells. *Int. J. Hydrogen Energy* **2021**, *46* (38), 20087−20092.

(10) Park, J.; Lee, Y.; Chang, I.; Cho, G. Y.; Ji, S.; Lee, W.; Cha, S. W. Atomic layer deposition of yttria-stabilized zirconia thin films for enhanced reactivity and stability of solid oxide fuel cells. *Energy* **2016**, *116*, 170−176.

(11) Mukai, T.; Tsukui, S.; Yoshida, K.; Yamaguchi, S.; Hatayama, R.; Adachi, M.; Ishibashi, H.; Kakehi, Y.; Satoh, K.; Kusaka, T.; Goretta, K. C. Fabrication of Y2O3-doped zirconia/gadolinia-doped ceria bilayer electrolyte thin film SOFC cells of SOFCs by single-pulsed laser deposition processing. *J. Fuel Cell Sci. Technol.* **2013**, *10* (6), No. 061006.

(12) Lee, Y. H.; Ren, H.; Wu, E. A.; Fullerton, E. E.; Meng, Y. S.; Minh, N. Q. All-sputtered, superior power density thin-film solid oxide fuel cells with a novel nanofibrous ceramic cathode. *Nano Lett.* **2020**, *20* (5), 2943−2949.
(13) Ren, H.; Lee, Y. H.; Wu, E. A.; Chung, H.; Meng, S. Y.; Fullerton, E. E.; Minh, N. Q. Nano-ceramic cathodes via co-sputtering of GdCe alloy and lanthanum strontium cobaltite for low temperature thin film solid oxide fuel cells. *ACS Appl. Energy Mater.* **2020**, *3*, 8135−8142.
(14) Tucker, M. C. Progress in metal-supported solid oxide fuel cells: A review. *J. Power Sources* **2010**, *195* (15), 4570−4582.
(15) Krishnan, V. V. Recent developments in metal-supported solid oxide fuel cells. *Wiley Interdiscip. Rev.: Energy Environ.* **2017**, *6* (5), No. e246.
(16) Xu, H.; Han, Y.; Zhu, J.; Ni, M.; Yao, Z. Status and progress of metal-supported solid oxide fuel cell: Towards large-scale manufactory and practical applications. *Energy Rev.* **2024**, *3* (1), No. 100051.
(17) Kim, K. H.; Park, Y. M.; Kim, H. Fabrication and evaluation of the thin NiFe supported solid oxide fuel cell by co-firing method. *Energy* **2010**, *35* (12), 5385−5390.
(18) Cho, H. J.; Kim, K. J.; Park, Y. M.; Choi, G. M. Flexible solid oxide fuel cells supported on thin and porous metal. *Int. J. Hydrogen Energy* **2016**, *41* (22), 9577−9584.
(19) Lee, K.; Kang, J.; Lee, J.; Lee, S.; Bae, J. Evaluation of metal-supported solid oxide fuel cells (MS-SOFCs) fabricated at low temperature (∼1,000 °C) using wet chemical coating processes and a catalyst wet impregnation method. *Int. J. Hydrogen Energy* **2018**, *43* (7), 3786−3796.
(20) Udomsilp, D.; Rechberger, J.; Neubauer, R.; Bischof, C.; Thaler, F.; Schafbauer, W.; Menzler, N. H.; de Haart, L. G. J.; Nenning, A.; Opitz, A. K.; Guillon, O.; Bram, M. Metal-supported solid oxide fuel cells with exceptionally high power density for range extender systems. *Cell Rep. Phys. Sci.* **2020**, *1* (6), No. 100072.
(21) Abdullaev, R. N.; Kozlovskii, Y. M.; Khairulin, R. A.; Stankus, S. V. Density and Thermal Expansion of High Purity Nickel over the Temperature Range from 150 to 2030 K. *Int. J. Thermophys.* **2015**, *36* (4), 603−619.
(22) Raju, S.; Sivasubramanian, K.; Divakar, R.; Panneerselvam, G.; Banerjee, A.; Mohandas, E.; Antony, M. P. Thermal expansion studies on Inconel-600 by high temperature X-ray diffraction. *J. Nucl. Mater.* **2004**, *325* (1), 18−25.
(23) Weimar, M. R.; Chick, L. A.; Gotthold, D. W.; Whyatt, G. A. In *Cost Study for Manufacturing of Solid Oxide Fuel Cell Power Systems*; Pacific Northwest National Lab. (PNNL): Richland, WA, 2013.
(24) Rossmeisl, J.; Bessler, W. G. Trends in catalytic activity for SOFC anode materials. *Solid State Ionics* **2008**, *178* (31−32), 1694−1700.
(25) Kashani, H.; Chen, M. Flaw-free nanoporous Ni for tensile properties. *Acta Mater.* **2019**, *166*, 402−412.
(26) Riyadi, T. W. B.; Setiadhi, D.; Anggono, A. D.; Siswanto, W. A.; Al-Kayiem, H. H. Analysis of mechanical and thermal stresses due to TiN coating of Fe substrate by physical vapor deposition. *Forces Mech.* **2021**, *4*, No. 100042.
(27) Wu, J.; Liu, X. Recent Development of SOFC Metallic Interconnect. *J. Mater. Sci. Technol.* **2010**, *26* (4), 293−305.
(28) Hayashi, H.; Saitou, T.; Maruyama, N.; Inaba, H.; Kawamura, K.; Mori, M. Thermal expansion coefficient of yttria stabilized zirconia for various yttria contents. *Solid State Ionics* **2005**, *176* (5−6), 613−619.
(29) Coaty, C.; Zhou, H.; Liu, H.; Liu, P. A Scalable Synthesis Pathway to Nanoporous Metal Structures. *ACS Nano* **2018**, *12* (1), 432−440.
(30) Feng, S.; Petrova, V.; Corrao, A. A.; Wang, S.; Yang, K.; Khalifah, P. G.; Liu, P. Morphological control of nanoporous copper formed from conversion reaction synthesis. *J. Phys. Chem. C* **2022**, *126* (35), 14878−14885.
(31) Kishimoto, H.; Suzuki, A.; Shimonosono, T.; Brito, M. E.; Yamaji, K.; Horita, T.; Munakata, F.; Yokokawa, H. Agglomeration behavior of nickel particles on YSZ and TiO2-doped YSZ electrolytes. *J. Power Sources* **2012**, *199*, 174−178.
(32) Yu, W.; Lim, Y.; Lee, S.; Pandiyan, A.; Cho, G. Y.; Cha, S. W. Low-temperature, high-performance thin-film solid oxide fuel cells with tailored nano-column structures of a sputtered Ni anode. *J. Mater. Chem. A* **2020**, *8* (41), 21668−21679.
(33) Solovyev, A. A.; Shipilova, A. V.; Rabotkin, S. V.; Smolyanskiy, E. A.; Shmakov, A. N. Magnetron sputtered LSC-GDC composite cathode interlayer for intermediate-temperature solid oxide fuel cells. *Int. J. Hydrogen Energy* **2022**, *47* (89), 37967−37977.
(34) Chiodelli, G.; Malavasi, L. Electrochemical open circuit voltage (OCV) characterization of SOFC materials. *Ionics* **2013**, *19* (8), 1135−1144.
(35) Lee, S.; Yu, W.; Jang, Y.; Ryu, S.; Hwang, J.; Cho, G. Y.; Ahn, D.-G.; Cha, S. W. Improved Reversibility of Thin-Film Solid Oxide Cells at 500 °C by Tailoring Sputtering Processes for Depositing Yttria-Stabilized Zirconia Electrolyte. *ACS Appl. Mater. Interfaces* **2024**, *16* (29), 37874−37884.
(36) Lee, H. Y.; Yu, W.; Lee, Y. H. High-performance low-temperature solid oxide fuel cell with nanostructured lanthanum strontium cobaltite/yttria-stabilized zirconia cathode via advanced co-sputtering. *J. Alloys Compd.* **2024**, *972*, No. 172740.
(37) Gil, D.; Jeong, I.; Lee, M. S.; Ko, S.; Jang, K. H.; Yu, W.; Cha, S. W. Impact of yttria-stabilized zirconia contents in nickel cermet anodes for intermediate temperature-operated syngas-fueled thin film solid oxide fuel cells. *Int. J. Hydrogen Energy* **2024**, *57*, 1408−1418.
(38) Noh, H.-S.; Hong, J.; Kim, H.; Yoon, K. J.; Kim, B.-K.; Lee, H.-W.; Lee, J.-H.; Son, J.-W. Scale-Up of Thin-Film Deposition-Based Solid Oxide Fuel Cell by Sputtering, a Commercially Viable Thin-Film Technology. *J. Electrochem. Soc.* **2016**, *163* (7), F613.
(39) Sumi, H.; Takahashi, S.; Yamaguchi, Y.; Shimada, H. Lanthanum-doped ceria interlayer between electrolyte and cathode for solid oxide fuel cells. *J. Asian Ceram. Soc.* **2021**, *9* (2), 609−616.
(40) Zhang, C.; Li, C.-J.; Zhang, G.; Ning, X.-J.; Li, C.-X.; Liao, H.; Coddet, C. Ionic conductivity and its temperature dependence of atmospheric plasma-sprayed yttria stabilized zirconia electrolyte. *Mater. Sci. Eng., B* **2007**, *137* (1), 24−30.
(41) Ryu, S.; Yu, W.; Tran, Q. T.; Thieu, C. A.; Lee, S.; Sreenarayanan, B.; Feng, S.; Meng, S.; Fullerton, E. E.; Liu, P.; Minh, N. Q. Fabrication of Low-Temperature Solid Oxide Fuel Cells via Development of Magnetron Sputtering Process. *ECS Trans.* **2023**, *111* (6), 707.
(42) Virkar, A. V.; Chen, J.; Tanner, C. W.; Kim, J.-W. The role of electrode microstructure on activation and concentration polarizations in solid oxide fuel cells. *Solid State Ionics* **2000**, *131* (1), 189−198.
(43) Shimada, H.; Suzuki, T.; Yamaguchi, T.; Sumi, H.; Hamamoto, K.; Fujishiro, Y. Challenge for lowering concentration polarization in solid oxide fuel cells. *J. Power Sources* **2016**, *302*, 53−60.

https://doi.org/10.1021/acsaem.4c02244
ACS Appl. Energy Mater. XXXX, XXX, XXX−XXX